On the nonlinear threshold versus distance in long-haul highly-dispersive coherent systems

A. Bononi,[*] **N. Rossi, and P. Serena**

Dip. Ing. informazione, Università degli Studi di Parma, Parma, Italy

[*]*alberto.bononi@unipr.it*

Abstract: We show that the accumulation rate of nonlinearity in highly-dispersive long-haul coherent links can also be measured from the nonlinear threshold decrease rate, and provide simulations of such rates for both single- and cross-channel effects. We then show how the estimated rate can be used for the overall system design.

© 2012 Optical Society of America

References and links

1. M. Nazarathy, J. Khurgin, R. Weidenfeld, Y. Meiman, P. S. Pak, R. Noe, I. Shpantzer, and V. Karagodsky, "Phased-array cancellation of nonlinear FWM in coherent OFDM dispersive multi-span links, " Opt. Express **16**(20), 4228–4236, (2008).
2. X. Chen and W. Shieh, "Closed-form expressions for nonlinear transmission performance of densely spaced coherent optical OFDM systems," Opt. Express **18**(18), 19039–19054 (2010).
3. G. Bosco, A. Carena, R. Cigliutti, V. Curri, P. Poggiolini, and F. Forghieri, "Performance prediction for WDM PM-QPSK transmission over uncompensated links," in *Proc. OFC 2011* (Los Angeles, CA, 2011). Paper OThO7.
4. P. Poggiolini, A. Carena, V. Curri, G. Bosco, and F. Forghieri, "Analytical modeling of non-linear propagation in uncompensated optical transmission links," IEEE Photon. Technol. Lett. **23**(11), 742–744 (2011).
5. E. Grellier, and A. Bononi, "Quality parameter for coherent transmissions with Gaussian-distributed nonlinear noise," Opt. Express **19**(13), 12781–12788 (2011).
6. A. Carena, V. Curri, G. Bosco, P. Poggiolini, and F. Forghieri, "Modeling of the impact of non-Linear propagation effects in uncompensated optical coherent transmission links," J. Lightwave Technol. **30**(10), 1524–1539 (2012).
7. A. Bononi, P. Serena, N. Rossi, E. Grellier, and F. Vacondio, "Modeling nonlinearity in coherent transmissions with dominant intrachannel-four-wave-mixing," Opt. Express **20**(7), 7777–7791 (2012).
8. F. Vacondio, O. Rival, C. Simonneau, E. Grellier, A. Bononi, L. Lorcy, J.-C. Antona, and S. Bigo, "On nonlinear distortions of highly dispersive optical coherent systems," Opt. Express **20**(2), 1022–1032 (2012).
9. A. Carena, G. Bosco, V. Curri, P. Poggiolini, M. Tapia Taiba, and F. Forghieri, "Statistical characterization of PM-QPSK signals after propagation in uncompensated fiber links," in *Proc. ECOC 2010* (Turin, Italy, 2010). Paper P4.07.
10. A. Bononi, P. Serena, N. Rossi, and D. Sperti, "Which is the dominant nonlinearity in long-haul PDM-QPSK coherent transmissions?," in *Proc. ECOC 2010* (Turin, Italy, 2010). Paper Th10E1.
11. O. V. Sinkin, J.-X. Cai, D. G. Foursa, H. Zhang, A. N. Pilipetskii, G. Mohs, and Neal S. Bergano, "Scaling of nonlinear impairments in dispersion-uncompensated long-Haul transmission," in *Proc. OFC 2012* (Los Angeles, CA, 2012). Paper OTu1A.
12. A. Bononi N. Rossi, and P. Serena, "Transmission limitations due to fiber nonlinearity," in *Proc. OFC 2011* (Los Angeles, CA, 2011). Paper OWO7.
13. O. Rival, and K. Mheidly, "Accumulation rate of inter and intra-channel nonlinear distortions in uncompensated 100G PDM-QPSK systems," in *Proc. OFC 2012* (Los Angeles, CA, 2012). Paper JW2A.52.
14. A. Bononi, N. Rossi, and P. Serena, "Nonlinear threshold decrease with distance in 112 Gb/s PDM-QPSK coherent systems," in *Proc. ECOC 2012* (Amsterdam, The Netherlands, 2012). Paper We.2.C.4.
15. J. C. Antona and S. Bigo, "Physical design and performance estimation of heterogeneous optical transmission systems," C. R. Physique **9**, 963–984 (2008).

16. Y. Frignac, J.-C. Antona, and S. Bigo, "Enhanced analytical engineering rule for fast optimization of dispersion map in 40 Gbit/s-based transmission systems," in *Proc. OFC 2004* (Los Angeles, CA, 2004). Paper TuN3.
17. A. Bononi, P. Serena, and A. Orlandini, "A unified design framework for single-channel dispersion-managed terrestrial systems," J. Lightwave Technol. **26**(22), 3617–3631 (2008).
18. A. Bononi, P. Serena, and N. Rossi, "Nonlinear signal-noise interactions in dispersion-managed links with various modulation formats," Opt. Fiber Technol. **16**(2), 73–85 (2010).
19. M. Winter, C.-A. Bunge, D. Setti, and K. Petermann, "A statistical treatment of cross-polarization modulation in DWDM systems," J. Lightwave Technol. **27**(17), 3739–3751 (2009).
20. "Optilux Toolbox," [Online]. Available http://www.optilux.sourceforge.net
21. J.-C. Antona, E. Grellier, A. Bononi, S. Petitreaud, and S. Bigo, "Revisiting binary sequence length requirements for the accurate emulation of highly dispersive transmission systems," in *Proc. ECOC 2008* (Brussels, Belgium, 2008). Paper We.1.E.3.
22. E. Grellier, J.-C. Antona, A. Bononi, and S. Bigo, "Revisiting binary sequence length requirements to accurately emulate optical transmission systems in highly dispersive regime," SPIE **7136**, 713613 (2008).
23. Y. Ye, L. N. Binh, E. Zhou, T. Wu, S. Zhang, and X. Xu, "A simple criterion for performance estimation of 112Gb/s PDM-QPSK WDM system over uncompensated links," in *Proc. OFC 2012* (Los Angeles, CA, 2012). Paper JW2A.45.
24. V. A. J. M. Sleiffer, M. S. Alfiad, D. van den Borne, S. L. Jansen, M. Kuschnerov, S. Adhikari, and H. De Waardt, "A comparison of 43-Gb/s POLMUX-RZ-DPSK and POLMUX-RZ-DQPSK modulation for long-haul transmission systems," in *Proc. ECOC 2010* (Turin, Italy, 2010). Paper Mo.2.C.4.
25. M. Salsi, C. Koebele, P. Tran, H. Mardoyan, S. Bigo, and G. Charlet, "80×100-Gbit/s transmission over 9,000km using erbium-doped fibre repeaters only," in *Proc. ECOC 2010* (Turin, Italy, 2010). Paper We.7.C.3.
26. E. Grellier, J.-C. Antona, and S. Bigo, "Revisiting the evaluation of non-linear propagation impairments in highly dispersive systems," in *Proc. ECOC 2009* (Vienna, Austria, 2009). Paper 10.4.2.
27. V. Curri, P. Poggiolini, G. Bosco, A. Carena, and F. Forghieri, "Performance evaluation of long-haul 100 Gb/s PM-QPSK transmission over different fiber types," IEEE Photon. Technol. Lett. **22**(19), 1446–1448 (2010).
28. P. Poggiolini, "The GN model of non-Linear propagation in uncompensated coherent optical systems," J. Lightwave Technol. (2012), Early Access.

---

1.   Introduction

A Gaussian nonlinear model (GNM) was recently introduced to justify the performance of dispersion uncompensated (DU) coherent links with orthogonal frequency division multiplexing signals [1,2] and with single-carrier signals [3–5]. According to that model, the nonlinear interference (NLI) is a signal-independent circular Gaussian noise, like the amplified spontaneous emission (ASE) noise. Thus performance just depends on the nonlinear signal to noise ratio (SNR)

$$S = \frac{P}{N_A + a_{NL}P^3} \tag{1}$$

where P is the power per channel, N_A is the ASE power, and $N_{NLI} = \text{Var}[f_{NLI}] = a_{NL}P^3$ is the variance of the NLI field f_{NLI}, which scales cubically with P through the NLI coefficient a_{NL}. In a system with N spans, the ASE power scales linearly with N, while the NLI field $f_{NLI} = \sum_{k=1}^{N} f_k$ is the sum of N random variables (RV) contributed by each span. The accumulation law of N_{NLI} with distance N was shown by a frequency-domain analytical model for a Nyquist-spaced wavelength division multiplexed (WDM) system (channel spacing Δf equal to the symbol rate R) to be approximately $N_{NLI} \propto N(1 + \alpha \log N)$ with α a system parameter [6], while a single-channel time-domain analytical model yielded a scaling law $N_{NLI} \propto N \log(kN)$ with k a system parameter [7]. Since the variance N_{NLI} of the NLI field scales as N^1 if the span contributions f_k are uncorrelated equal-variance RVs, or as N^2 if the span contributions are the same RV, a pragmatic approximation to the distance scaling law assumes [8]

$$a_{NL} = \alpha_{NL}N^{1+\varepsilon} \tag{2}$$

with ε a system factor, whose value reasonably is between 0 and 1, and α_{NL} is a constant. The exponent was measured from experimental bit error rate (BER) measures as $1 + \varepsilon \cong 1.37$

in 50 GHz spaced, 28 Gbaud polarization division multiplexed quadrature phase shift keying (PDM-QPSK) channels over standard single mode fiber (SMF) DU links with 100 km spans and 80 WDM channels, and the fit was over the range $5 < N < 30$ [8]. For the same system, a value $1 + \varepsilon \cong 1.25$ over the larger $5 < N < 50$ can be read off the simulation results in [9]. The decrease of ε in such systems when the range of N is extended is confirmed by the single-channel analysis and simulations in [7]. Such WDM DU systems have a bandwidth fill-factor $\eta = \frac{R}{\Delta f} = 0.56$ and the dominant nonlinear effect is single channel self-phase modulation [10]. Recent experiments [11] performed on ultra-long DU SMF links with $\sim$50 km spans at variable η confirm that when $\eta \lesssim 0.6$ the NLI accumulation exponent is $1 + \varepsilon \cong 1.2 \div 1.6$ (since single-channel nonlinear effects are dominant [12]), while at larger η (where cross-nonlinearity starts to dominate) the exponent decreases to $1 + \varepsilon \cong 1.05$. A recent simulation study on 28 Gbaud PDM-QPSK transmission over an Nx100 km SMF DU link [13] found that the NLI coefficient a_{NL} can be approximated as the sum of single and cross-channel effects as $a_{NL} = \alpha_{SPM} N^{1.34} + \alpha_{XPM} N^{1.1}$ in the range $8 < N < 30$, where α_{XPM} increases for decreasing channel spacing Δf and eventually gives the dominant contribution as a unity fill-factor and thus the smallest spacing $\Delta f = R$ is approached, thus indirectly confirming the above experimental findings.

In this paper, which is an extended version of [14], we want to add to the debate by taking a correlated but different point of view. We already showed by simulation how the nonlinear threshold (NLT) at 1dB of SNR penalty $\hat{P}_1$ (i.e., the channel power at which a target bit error rate $BER_0 = 10^{-3}$ is obtained with 1 dB extra SNR with respect to linear propagation [15]) scales with symbol rate R at fixed bandwidth fill-factor η and at fixed distance N [10, 12]. We now wish to check by simulation how $\hat{P}_1$ scales with distance N at a fixed symbol rate and fixed η. The reason is that, as we will see, the GNM theory for DU systems predicts that the plot of NLT versus N in a log-log scale decreases with slope $-(1+\varepsilon)/2$ dB/dB. We wish to estimate the slope factor ε from our NLT simulations, and relate it to the ultimate system performance.

The paper is organized as follows. Sections 2-3 report on simulations of $\hat{P}_1$ versus distance (i.e., versus spans N) at a fixed symbol rate $R = 28$ Gbaud and Δf=50 GHz ($\eta = 0.56$) for a homogeneous WDM PDM-QPSK system over a Nx50 km SMF DU link, and we compare it to the one obtained with standard in-line dispersion management (DM). We use the nonlinear effects separation procedure [10] to estimate the slope at which the NLT due to individual self- and cross-nonlinear effects decreases at increasing N in both DU and DM systems. Section 4 finally provides a comprehensive view of the system implications of the 1dB NLT $\hat{P}_1$ and of the slope parameter ε.
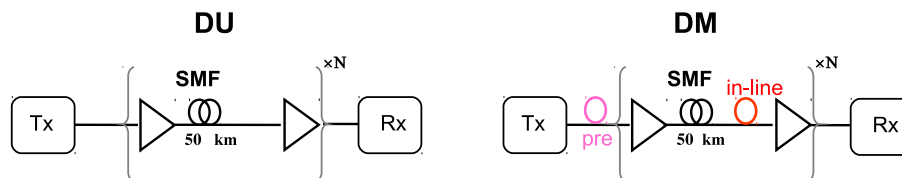
2. Simulated DU and DM systems

Fig. 1. Block diagrams of DU and DM simulated systems. TX block represents 19 WDM channels spaced by $\Delta f = 50$GHz, and NRZ-PDM-QPSK modulated at $R = 28$ Gbaud. In DM we use a residual dispersion per span of 30 ps/nm and distance-dependent pre-compensation (3). Propagation uses the SSFM with Manakov nonlinear step.

Figure 1 shows the block diagram of the simulated DU and DM links. The transmitter con-

sisted of 19 WDM non-return to zero (NRZ) 28 Gbaud PDM-QPSK channels, with $\Delta f = 50$ GHz. All channels were modulated with 2^{10} and 2^{14} independent random symbols in the DM and DU cases, respectively. Each channel was filtered by a supergaussian filter of order 2 with bandwidth $0.9R$. The state of polarization (SOP) of each carrier was randomized on the Poincaré sphere. The transmission line consisted of N spans of 50km of SMF ($D = 17$ ps/nm/km, $\alpha = 0.2$ dB/km, $\gamma = 1.3$ W^{-1}km^{-1}). Propagation used the vector split-step Fourier method (SSFM) with zero polarization mode dispersion and Manakov nonlinear step [10]. In the DM case, an in-line residual dispersion per span (RDPS) of 30 ps/nm and a straight-line rule precompensation [16, 17]

$$D_{pre} = -\frac{D}{\alpha} - \frac{N-1}{2}RDPS \tag{3}$$

were used. In the coherent receiver we neglected laser phase noise and frequency offset. The standard digital signal processor consisted of a chromatic dispersion compensation block, of a data-aided polarization demultiplexer, and a 27 taps Viterbi and Viterbi phase estimator.

The objective of the simulations was to estimate the 1 dB NLT $\hat{P}_1$ versus distance when nonlinearities (NL) are selectively activated [10]. The NLT $\hat{P}_1$ is obtained from a series of BER Monte Carlo estimations (averaged over input polarization states) at increasing amplifiers noise figure until the target BER_0 is obtained, as detailed in [18]. In the DU case, noise was all loaded at the receiver since it is known that signal-noise nonlinear interactions are negligible at 28 Gbaud [18]. In the DM case we calculated the NLT both with distributed noise and with noise loading. Using nonlinearity decoupling, we studied the following four cases: 1) single channel (label "SPM" in the following figures); 2) WDM with only scalar XPM [19] active (label "XPM"); 3) WDM with only cross-polarization modulation [19] (label "XPolM") active; 4) WDM with all nonlinearities active (label "WDM").

Simulations were run using the open-source software Optilux [20]. Obtaining the curves presented in each subplot of the following Fig. 2 took approximately 3 weeks by running full time on an 8-core Dell workstation.
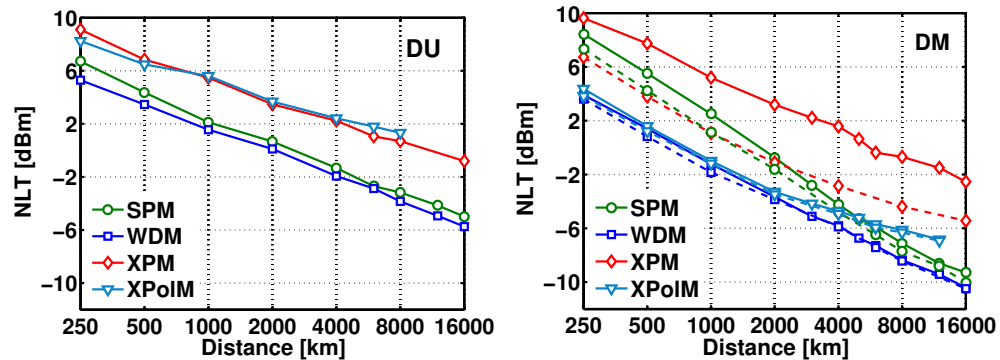
3. Results

Fig. 2. 1 dB NLT $\hat{P}_1$ at reference $BER_0 = 10^{-3}$ vs distance for 19-channel homogeneous 28 Gbaud NRZ PDM-QPSK system with $\Delta f = 50$ GHz over an Nx50 km SMF link. No PMD. (a) DU; (b) DM with 30 ps/nm RDPS and distance-dependent SLR precompensation (3); Solid lines: ASE noise loading at RX. Dashed lines: distributed ASE.

DU system. Figure 2(a) shows the corresponding NLT $\hat{P}_1$ versus distance, with span number N ranging from 5 to 320. We first remark that at all distances single-channel effects

(SPM) dominate at this $\eta = 0.56$ bandwidth fill-factor [12]. The effect of the comparable-size cross-nonlinearities XPM and XPolM on the overall NLT (WDM) is felt only at distances below 2000 km. The reason is that single-channel nonlinearity accumulates at a faster rate than cross-channel nonlinearity so that at longer distances it becomes largely dominant. Equation (18) predicts on this log-log plot a NLT decrease with a slope $-(1+\varepsilon)/2$ dB/dB. From Fig. 2 (a) on the narrow-range up to 2000 km (40 spans) by least mean-square fitting data with straight lines we find $\varepsilon_{SPM} \cong 0.32$, $\varepsilon_{XPM} \cong 0.22$, $\varepsilon_{XPolM} \cong -0.08$ and $\varepsilon_{WDM} \cong 0.16$, while fitting on the wide-range (up to 320 spans) we measure $\varepsilon_{SPM} \cong 0.28$, $\varepsilon_{XPM} \cong 0.08$, $\varepsilon_{XPolM} \cong -0.08$ and $\varepsilon_{WDM} \cong 0.22$. We first note that the wide-range ε_{WDM} value is consistent with measurements in [11] at similar η, while the narrow-range ε_{SPM} is in agreement with [13]. However, the most novel piece of information we learn from Fig. 2 is that the smaller slope of cross-nonlinearity observed in [13] is indeed an average of the XPolM and scalar XPM slopes, where scalar XPM seems to accumulate at a slightly faster rate. However, in DU links the rate difference is small. The negative measured ε_{XPolM} is ascribed to an insufficient pattern length, as discussed below.

DM system. It is instructive to also take a look at the NLT curves when the DU link is changed into a legacy DM link. Figure 2(b) shows both the unrealistic case of noise loading (solid lines) and the realistic case of ASE distributed at each amplifier, where nonlinear signal-ASE interactions are fully accounted for (dashed lines). We remark that pre-compensation is here *changed at each value of N* according to (3), hence the measured NLTs do not truly portray the noise accumulation with *N* in the *same* line. Figure 2(b) confirms that [12]:

i) scalar XPM plays a minor role in the PDM-QPSK constant intensity format, and is quite sensitive to signal-noise interactions, here manifested as nonlinear phase noise (NLPN);

ii) single channel (SPM) effects also play a minor role up to about 4000 km, and in that range are also quite sensitive to NLPN;

iii) the dominant nonlinearity is XPolM up to about 4000 km, but eventually SPM effects become dominant as they accumulate at a faster rate. XPolM is not impacted by signal-ASE interactions.

We note that the slope of SPM in the first 2000 km gives about $\varepsilon_{SPM} \cong 1$, but such a slope decreases at larger distances, since the RDPS starts contributing enough cumulated dispersion to make the DM system look more similar to a DU system. Within the first $\sim$2000 km we also measure (with NLPN) $\varepsilon_{XPM} \cong 0.73$ and $\varepsilon_{WDM} \cong 0.66$. The fact that XPolM is less "resonant" than scalar XPM is seen in the lowering of the local XPolM slope after 2000 km. The intuitive reason of XPolM's smaller slope is easily understood in a truly resonant DM map (i.e., with RDPS=0). In such a case the walkoff completely realigns the interfering pattern intensities, hence scalar XPM is identical at each span, i.e., it is truly resonant. Instead, the rotations induced by XPolM never bring back the final SOP to the same starting SOP at each span, hence XPolM is never truly resonant.

XPolM pattern dependence. The choice of the modulating pattern sequence length is of great importance in establishing the XPolM NLT. Note that in this study we did not use pseudo-random patterns, but completely random patterns which – at equal accuracy – allow the use of shorter pattern lengths and are thus more appropriate in simulations of DU systems [21, 22]. Figure 3 reports on the pattern length sensitivity of the XPolM NLT $\hat{P}_1$ vs. distance for the same DU and DM systems analyzed in Fig. 2. If the sequence length is too short, the XPolM $\hat{P}_1$ slope erroneously decreases at increasing distance. We found that a length of 2^{10} symbols was sufficient for our DM systems, while for DU systems we used the longest 2^{14} sequence length that allowed us to obtain the 1dB NLT curves in a feasible time, although still longer sequences may probably be needed in order to precisely estimate the XPolM NLT slope.
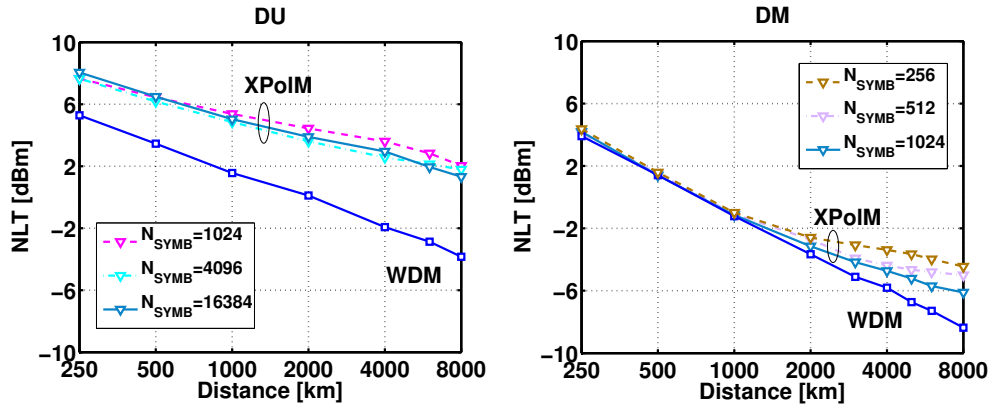
Fig. 3. XPolM NLT $\hat{P}_1$ vs. distance for same 19-channel WDM DU (a) and DM (b) systems as in Fig. 2, for several values of the number of random symbols in the SSFM.
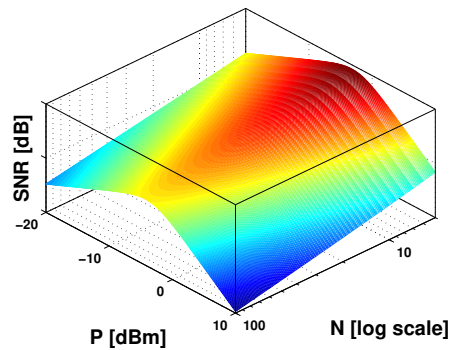

Fig. 4. Qualitative example of 2-dimensional SNR surface [dB] versus both power P [dBm] and number of spans N (logarithmic scale).

Although the distinction between XPM and XPolM is fundamental in practice for DM systems, for DU systems it tends to get blurred, and since XPM and XPolM are correlated, in the end what matters is their joint variance, as recently studied in [6].

4. System implications of slope parameter and NLT

According to the GNM, the nonlinear SNR Eq.(1) uniquely determines the value of bit error rate or equivalently of Q-factor [5]. Hence the surface of SNR versus power and spans contains all the needed information about global system performance. Figure 4 provides an example of the SNR surface in dB, S^{dB}, versus power P^{dB} and number of spans N^{dB} (for any variable x, we will denote $x^{dB} = 10\mathrm{Log}(x)$). It is the objective of this section to summarize the analytical properties of such a surface and explain how the exponent ε and the $\hat{P}_1$ vs. N curves fit into such a global view. Section 4.1 describes the properties of the "vertical cuts" S vs. P at a fixed distance N, known as the "bell curves". Section 4.2 describes the properties of the "horizontal cuts" P vs. N at a desired level S_0, tackling the issue of maximum transmission distance. Note that according to the models in [6,7] the NLI coefficient a_{NL} depends on the modulation format only through its symbol rate. Hence, by varying S_0, one finds the performance of any zero-mean format at a given symbol rate.
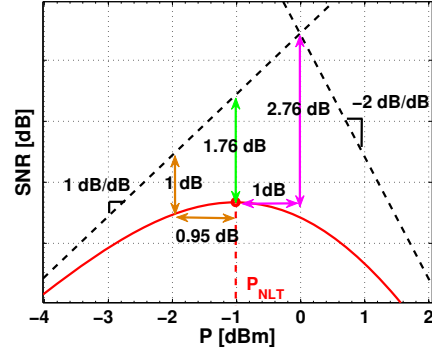
Fig. 5. SNR versus P at distance N. At 1dB above NLT, ASE has same power as NLI.

4.1. Vertical cuts: the bell curves

We wish to summarize here the behavior of S versus P at a fixed distance N. More information can be found in [3,5]. We first notice from Eq. (1) two asymptotes, one at small power $S_L \triangleq \frac{P}{N_A}$ which is the linear SNR, and one at large power $S_R \triangleq \frac{1}{a_{NL}P^2}$. The two asymptotes cross at the break-point power $P_B = \left(\frac{N_A}{a_{NL}}\right)^{\frac{1}{3}}$ where ASE power equals nonlinear noise power. The linear asymptote has slope 1 dB/dB, while the nonlinear asymptote has slope -2 dB/dB. Figure 5 shows SNR versus P for fixed values of ASE power N_A and nonlinearity a_{NL} where the two asymptotes are indicated by dashed lines. Equation (1) can be rearranged as

$$SP = \frac{S_L}{S} = 1 + \frac{a_{NL}P^3}{N_A} \tag{4}$$

where SP is the sensitivity penalty in linear units, and in dB it is the distance of the SNR curve from the linear asymptote S_L, as seen in Fig. 5.

4.1.1. Unconstrained nonlinear threshold

The unconstrained nonlinear threshold (NLT) is defined as the power P_{NLT} that maximizes the bell curve. By setting $\frac{dS}{dP} = 0$ we see that the NLT satisfies $N_A = 2(a_{NL}P^3)$, i.e., at the optimal power ASE noise is twice the nonlinear noise, and the SP is $(\frac{3}{2})^{dB} \sim 1.76$ dB [3–5] and this is true for all GNM systems. Explicitly,

$$P_{NLT} = \left(\frac{N_A}{2a_{NL}}\right)^{\frac{1}{3}} \tag{5}$$

and this is exactly 1 dB below the break-point P_B. The corresponding maximum SNR is:

$$S_{NLT} = \left(3^3 a_{NL}(\frac{N_A}{2})^2\right)^{-\frac{1}{3}} \equiv \frac{P_{NLT}}{\frac{3}{2}N_A}. \tag{6}$$

Since at NLT the penalty is 1.76 dB, it is interesting to ask at which power P_y we reach a penalty of y^{dB}. The answer is found by imposing $SP = 10^{y^{dB}/10}$ and rearranging Eq. (4): $P_y = P_{NLT} \cdot [2(10^{y^{dB}/10} - 1)]^{1/3}$. For instance, P_1^{dB} is 0.95 dB below P_{NLT}^{dB}, as also marked in Fig. 5.
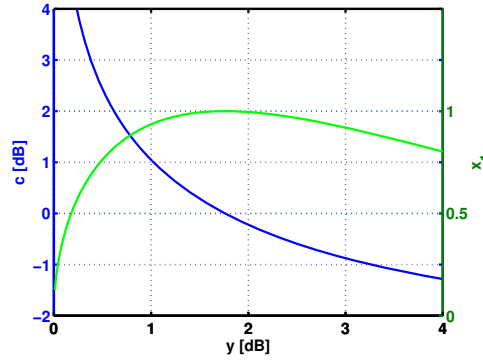
Fig. 6. $c \triangleq \hat{P}_{NLT}/\hat{P}_y$ [dB] (left axis) and $x = N_A/\hat{N}_A$ (right axis) versus penalty y^{dB}.

4.1.2. Constrained NLT

Given a desired SNR level S_0, it was shown in ([7] Appendix 1 and Fig. 3) that the bell curve reaches its top level at value S_0 when ASE power is $\hat{N}_A = \frac{2}{(3S_0)^{3/2}a_{NL}^{1/2}}$ and signal power is

$$\hat{P}_{NLT} = \frac{3}{2}S_0\hat{N}_A = \frac{1}{\sqrt{3S_0 a_{NL}}} \qquad (7)$$

which we call the *constrained NLT* at S_0. When $N_A < \hat{N}_A$, the SNR S exceeds S_0 over the whole range $P_m < P < P_M$, where

$$
\begin{aligned}
P_M &= 3S_0\hat{N}_A \cos\left(\frac{\arccos(-N_A/\hat{N}_A)}{3}\right) \\
P_m &= 3S_0\hat{N}_A \cos\left(\frac{2\pi-\arccos(-N_A/\hat{N}_A)}{3}\right).
\end{aligned}
\qquad (8)
$$

When instead $N_A > \hat{N}_A$, the target S_0 is unachievable. The penalty corresponding to the extremes P_m, P_M is found as $SP_{m,M} = \frac{P_{m,M}}{N_A S_0}$, since $S_0 N_A$ is the required minimal power to achieve S_0 in the linear regime. Figure 3(b) in [7] shows a plot of $SP_{m,M}$ versus power. When $P_m \equiv P_M$ we know the SP with respect to S_0 is 1.76 dB. For any other SP value y^{dB}, it is also interesting to find the power $\hat{P}_y$ (i.e., either P_m when $y^{dB} < 1.76$, or P_M when $y^{dB} > 1.76$.) achieving $SP = y^{dB}$. We call $\hat{P}_y$ the *constrained NLT* at y^{dB} of penalty. Defining

$$c(y^{dB}) \triangleq \hat{P}_{NLT}/\hat{P}_y \qquad (9)$$

we already showed in [7] that $c(1) = 1.27$, hence the constrained 1dB NLT $\hat{P}_1$ is 1.04 dB below $\hat{P}_{NLT}$ (while we have seen that the unconstrained P_1 is 0.95 dB below the unconstrained P_{NLT}).

The whole $c(y^{dB})$ curve can be obtained as follows. Let $SP = 10^{y^{dB}/10}$ and $x = N_A/\hat{N}_A \in [0,1]$, and look for the solution of the nonlinear equation $SP = \frac{3}{x}\cos\left(\frac{2\pi-\arccos(-x)}{3}\right)$ when $y^{dB} \le 1.76$, and of $SP = \frac{3}{x}\cos\left(\frac{\arccos(-x)}{3}\right)$ when $y^{dB} > 1.76$. Once x is found, calculate $c(y^{dB}) = 3/(2x \cdot 10^{y^{dB}/10})$. The result is plotted in Fig. 6. In blue we show the dB value of the curve $c(y^{dB})$, which is zero at $y^{dB} = 1.76$, while in green we show the curve $x(y^{dB})$.

4.2. *Horizontal cuts*

ASE in dual polarization systems accumulates as $N_A = \beta N$, where $\beta = h\nu FGB_{RX}$ depends on photon energy $h\nu$ at signal frequency ν, amplifiers noise figure F, gain G, and two-sided
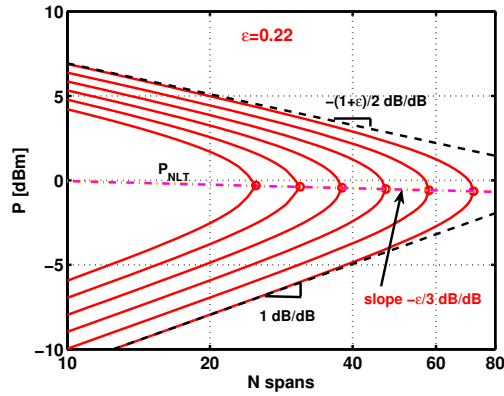
Fig. 7. Set of horizontal cuts of SNR surface $S(N,P)$ at levels $S_0 = [10.12 : 1 : 15.12]$ dB, for a DU Nx50km SMF link at 28Gbaud. Parameters: $\alpha_{NL} = 3.95 \cdot 10^{-4}$ [mW^{-2}], $\varepsilon = 0.22$, $F = 13$ dB, $B_{RX} = 32.5$ GHz. Locus of maxima (P_0, N_0) for varying S_0 shown as dash-dotted magenta line with slope $-\varepsilon/3 \cong -0.07$ dB/dB.

receiver noise bandwidth B_{RX}. We now assume for a_{NL} a simplified distance scaling law as in Eq. (2) and want to check the impact of the exponent factor ε.

Figure 7 shows a set of horizontal cuts of the SNR surface $S(N,P)$ at levels S_0 spaced by 1 dB. In the figure we assumed $\varepsilon = 0.22$. The analytical shape of each contour is obtained from

$$S_0 = \frac{P}{\beta N + \alpha_{NL} N^{1+\varepsilon} P^3} \tag{10}$$

which yields the explicit contour equation P versus N. The two solutions of the cubic Eq. (10) are the powers P_M (top branch up to the red circle) and P_m (bottom branch) whose analytical expression is given in Eq. (8). Each contour level has two asymptotes, obtained by suppressing either ASE or NLI in Eq. (10):

i) a lower (or linear) asymptote which in dB is a straight line with positive slope 1dB/dB:

$$P_L = LT_1 \cdot N \tag{11}$$

where we defined the "linear threshold"

$$LT_1 = \beta S_0 \tag{12}$$

as the power achieving S_0 at 1 span in the linear regime;

ii) a higher asymptote:

$$P_H = (S_0 a_{NL})^{-1/2} \tag{13}$$

which, in the simplifying assumption Eq. (2), in dB is a straight line with negative slope $-(1+\varepsilon)/2$. Only the asymptotes for the lowest contour level are marked in Fig. 7.

4.2.1. Unconstrained NLT

Consider the magenta-line locus of points of maximum reach (N_0, P_0) at each S_0 level, marked with red circles in Fig. 7. Information on how (N_0, P_0) change with S_0 is useful to understand the effect of the modulation format: at a given symbol rate, in general different formats will require different SNR S_0 to reach a desired target Q-factor Q_0 or BER value BER_0. It is thus important to understand by how much maximum distance and optimal power change as the modulation

format is changed. The points (N_0, P_0) are such that $P_m \equiv P_M$, i.e., they correspond to a distance N_0 where power P_0 coincides with $\hat{P}_{NLT}$, the constrained NLT at S_0. Therefore each red circle corresponds to the top of the "vertical cut" at N_0. In other words, the magenta-line is the "crest" of the S surface, or equivalently the locus of the *unconstrained NLT* P_{NLT} as N varies. As such, given N_0, we have from Eq. (5), Eq. (6):

$$P_0 = \left(\frac{\beta}{2\alpha_{NL} N_0^\varepsilon} \right)^{\frac{1}{3}} \quad ; \quad S_0 = \left(3^3 \alpha_{NL} N_0^{3+\varepsilon} \left(\frac{\beta}{2}\right)^2 \right)^{-\frac{1}{3}} \equiv \frac{P_0}{\frac{3}{2}\beta N_0}. \tag{14}$$

The first equation in Eq. (14) shows that the magenta line has a slope of $-\frac{\varepsilon}{3}$ dB/dB [11]. With the value for SPM-dominated DU systems of $\varepsilon = 0.22$ found by simulations in Fig. 2(a), this slope is -0.07 dB/dB, which is hardly noticeable in lab experiments, so that common wisdom has that in DU systems the unconstrained NLT does not depend on distance, as experimentally verified by many authors, see e.g. [11, 24].

The second equation in Eq. (14) shows that the "crest" of surface S^{dB} versus N_0 is a straight line with slope $-\frac{3+\varepsilon}{3} \sim -1$ dB/dB as for linear systems, as experimentally verified in [25].

The crest is obtained when ASE power is 2 times the NLI power. However, one can similarly prove that the locus of points where ASE power is k times the NLI power at coordinate N_k satisfies

$$P_k = \left(\frac{\beta}{2\alpha_{NL} N_k^\varepsilon} \right)^{\frac{1}{3}} \quad ; \quad S = \frac{P_k}{\frac{k+1}{k} N_A} = \left((k+1)^3 \alpha_{NL} N_k^{3+\varepsilon} \left(\frac{\beta}{k}\right)^2 \right)^{-\frac{1}{3}} \tag{15}$$

which proves that the whole S^{dB} surface sketched in Fig. 4 is composed of parallel straight-lines.

4.2.2. Constrained NLT

Using Eq. (2) in Eq. (7) we have

$$\hat{P}_{NLT} = NLT_1 \cdot N^{-\frac{1+\varepsilon}{2}} \tag{16}$$

where we defined the effective 1-span constrained NLT power as

$$NLT_1 \triangleq (3S_0 \alpha_{NL})^{-\frac{1}{2}}. \tag{17}$$

Since the higher asymptote Eq. (13) can be also expressed as $P_H = \sqrt{3} NLT_1 \cdot N^{-\frac{1+\varepsilon}{2}}$, then it is clear that the dB-dB plot of $\hat{P}_{NLT}$ versus N is a straight line parallel to P_H but lowered by $\sqrt{3} \sim 2.38$ dB, as shown by the magenta dash-dotted line in Fig. 8. Similarly, from Eq. (9) and using Eq. (16) we also have

$$\hat{P}_y = \frac{NLT_1}{c(y^{dB})} N^{-\frac{1+\varepsilon}{2}} \tag{18}$$

where $c(y^{dB})$ is shown in Fig. 6. A similar scaling law was already reported in [23] for DU systems with $\varepsilon = 0$. Hence for instance $\hat{P}_1$ is a straight line parallel to $\hat{P}_{NLT}$ but lowered by ~ 1.04 dB as reported in blue solid line in Fig. 8. The parameters NLT_1 and ε used in the figure were obtained by straight-line fitting the simulated $\hat{P}_1$ vs. N "WDM" curve in Fig. 2(a).

Note that Eq. (16) can be rearranged as

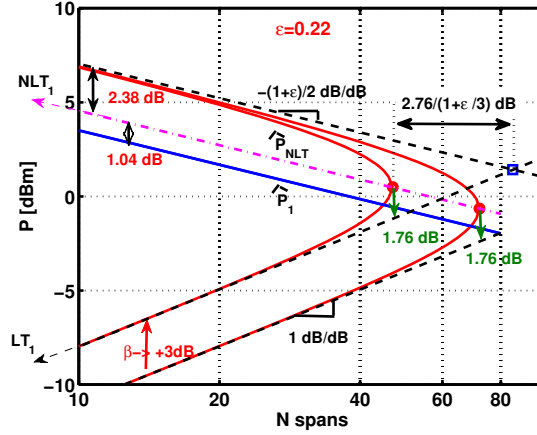$$N\hat{P}_{NLT}(N) = NLT_1 \cdot N^{\frac{1-\varepsilon}{2}}. \tag{19}$$

Fig. 8. Horizontal cut of SNR surface $S(N,P)$ at level $S_0 = 10.12$ dB ($BER_0 = 10^{-3}$ for the PDM-QPSK receiver used in simulations) for DU Nx50km SMF link at 28 Gbaud, for 2 values of ASE factor β spaced by 3dB. Parameters: $\alpha_{NL} = 3.95 \cdot 10^{-4}$ [mW^{-2}], $\varepsilon = 0.22$ chosen such that the blue line $\hat{P}_1$ is the least-mean-squares fit of the simulated "WDM" 1dB NLT (at the same $S_0 = 10.12$ dB) in Fig. 2(a). Other parameters $F = [13, 16]$ dB, $B_{RX} = 32.5$ GHz. Upper and lower asymptotes P_H and P_L shown as dashed black lines. Locus of maxima (P_0, N_0) for varying β (i.e. $\hat{P}_{NLT}$) shown as dash-dotted magenta line parallel to P_H, shifted downwards by $10\text{Log}\sqrt{3} = 2.38$ dB (cfr Eq. (17)). The 1dB NLT $\hat{P}_1$ (blue, solid) is parallel to $\hat{P}_{NLT}$, and located $c = 1.04$ dB below (c values at other penalties are found in Fig. 6). Maxima are $10\text{Log}(3/2) = 1.76$ dB from lower asymptote (green arrows). At $N = 1$, have $P_L \equiv LT_1$ and $\hat{P}_{NLT} \equiv NLT_1$.

The left-hand side is often called the integrated NLT, and its slope versus N was measured in ([26], Fig. 1) to be ~ 0.31 dB/dB for a 50 GHz spaced 28 Gbaud PDM-QPSK system over an Nx100 km DU SMF link, consistently with the experimentally estimated value $\varepsilon \sim 0.37$ [8].

Figure 8 shows that the magenta dash-dotted line is also the locus of maximum-reach points of coordinates (P_0, N_0) as the β factor (i.e., amplifiers noise figure for instance) is varied. This was already proven in [5], and it makes sense, since the $\hat{P}_1$ is obtained in simulations by varying the received ASE until 1 dB of penalty is measured. Similarly, the locus of maximum distance points (P_0, N_0) as the α_{NL} factor is varied with β held constant is a straight line parallel to the linear asymptote and 1.76 dB above it, since from Eq. (14) we have $P_0 = \frac{3}{2}\beta S_0 N_0 \equiv \frac{3}{2}P_L$. Figure 4 in [27] confirms this fact. The explicit expression of the constrained maximum distance N_0 is obtained from the two relations in Eq. (14) as

$$N_0 = \left((3S_0)^3 \alpha_{NL} \left(\frac{\beta}{2}\right)^2 \right)^{\frac{-1}{3+\varepsilon}} \equiv \left(\frac{NLT_1}{\frac{3}{2}LT_1} \right)^{\frac{2}{3+\varepsilon}} \tag{20}$$

and its associated "optimal" power as

$$P_0 = \left(\frac{\beta}{2}\right)^{\frac{1+\varepsilon}{3+\varepsilon}} (3S_0)^{\frac{\varepsilon}{3+\varepsilon}} \alpha_{NL}^{-\frac{1}{3+\varepsilon}} \equiv (NLT_1)^{\frac{2}{3+\varepsilon}} \left(\frac{3}{2}LT_1\right)^{\frac{1+\varepsilon}{3+\varepsilon}}. \tag{21}$$

If we look instead at the coordinates (N_0^A, P_0^A) of the point where the asymptotes cross, we find $N_0^A/N_0 = \left(\frac{\sqrt{3}}{2/3}\right)^{\frac{2}{3+\varepsilon}}$ and $P_0^A/P_0 = \left(2(2/3)^\varepsilon\right)^{\frac{1}{3+\varepsilon}}$. Hence if we judge the maximum distance

from the asymptotes we over-estimate the true N_0 by $2.76/(1+\varepsilon/3)$ dB and the true P_0 by $(3-1.76\varepsilon)/(3+\varepsilon)$ dB, as seen in Fig. 8.

Equations (20),(21) have two important consequences:

i) Sensitivity. By differentiating Eq. (20), Eq. (21) we immediately get

$$
\begin{cases}
\dfrac{\partial N_0^{dB}}{\partial S_0^{dB}} = -\dfrac{3}{3+\varepsilon} \\[4pt]
\dfrac{\partial N_0^{dB}}{\partial \beta^{dB}} = -\dfrac{2}{3+\varepsilon} \\[4pt]
\dfrac{\partial N_0^{dB}}{\partial \alpha_{NL}^{dB}} = -\dfrac{1}{3+\varepsilon}
\end{cases}
\qquad
\begin{cases}
\dfrac{\partial P_0^{dB}}{\partial S_0^{dB}} = \dfrac{\varepsilon}{3+\varepsilon} \\[4pt]
\dfrac{\partial P_0^{dB}}{\partial \beta^{dB}} = \dfrac{1+\varepsilon}{3+\varepsilon} \\[4pt]
\dfrac{\partial P_0^{dB}}{\partial \alpha_{NL}^{dB}} = -\dfrac{1}{3+\varepsilon}
\end{cases}
\tag{22}
$$

i.e., the sensitivity to changes in S_0 (e.g. modulation format or coding), β (e.g. amplifiers noise figure) and α_{NL} (e.g. fiber parameters such as nonlinearity and dispersion). Such changes need not be small, since the surface is made of straight lines. For instance, from the top left relation we see that if a more powerful code lowers the SNR S_0 by 1dB (without appreciably increasing the symbol rate), maximum distance is extended by $\frac{3}{3+\varepsilon}$ dB and the most beneficial case is $\varepsilon = 0$. The top right relation tells us that P_0 is very weakly dependent on SNR S_0, hence on modulation format. We can also use the middle relations Eq. (22) to conclude that in Fig. 8 when β is doubled (+3dB), the optimal power P_0 is increased by $\frac{3+3\varepsilon}{3+\varepsilon}$ dB (1.13 dB in figure), while maximum distance N_0 is decreased by $\frac{6}{3+\varepsilon}$ dB (1.86 dB in figure). The relations in the last line tell us that a 1dB increase in α_{NL} brings about a modest decrease by less than 1/3 dB in both N_0 [28] and P_0. It is the same decrease for both N_0 and P_0, since the optimal (N_0, P_0) in this case slides along a 1 dB/dB straight line parallel to the lower asymptote, as we already remarked.

ii) Power budget. It is simple to verify from the asymptotes that

$$
\frac{N_0^A}{N} = \left(\frac{P_H(N)}{P_L(N)} \right)^{\frac{2}{3+\varepsilon}}.
\tag{23}
$$

Hence the maximum extra distance N_0^A/N predicted from the asymptotes only depends on the "power budget" $P_H(N)/P_L(N)$, corresponding to the vertical dB spread of the contour at S_0 between the asymptotes at N. Similarly, Eq. (20) tells us that maximum reach N_0 at S_0 only depends on the power budget $\frac{NLT_1}{\frac{3}{2}LT_1}$, i.e., the vertical spread of the contour at S_0 at $N = 1$ span from 1.76 dB above the lower linear asymptote $P_L(1) = LT_1$ up to the magenta dash-dotted line $\hat{P}_{NLT}(1) = NLT_1$. Also, by using the second form of Eq. (20) and Eq. (19) one can estimate the extra distance ratio N_0/N from the *measured* value of the constrained NLT $\hat{P}_{NLT}(N)$ at S_0 at given distance N as

$$
\frac{N_0}{N} = \left(\frac{\hat{P}_{NLT}(N)}{\frac{3}{2}P_L(N)} \right)^{\frac{2}{3+\varepsilon}}
\tag{24}
$$

which only depends on the local power budget $\hat{P}_{NLT}(N)/(\frac{3}{2}P_L(N))$.

Finally, by checking the constrained NLT ratio of two different formats A and B at a common BER_0 (hence at possibly different $S_{0,A}$, $S_{0,B}$) one can estimate by how much the best format extends the maximum reach from:

$$
\frac{N_{0,A}}{N_{0,B}} = \left((\frac{\hat{P}_{NLT,A}(N)}{\hat{P}_{NLT,B}(N)}) / (\frac{LT_{1,A}}{LT_{1,B}}) \right)^{\frac{2}{3+\varepsilon}}
\tag{25}
$$

where $\frac{LT_{1,A}}{LT_{1,B}}$ is the ratio of sensitivities (at BER_0) of the two formats in the linear regime. Clearly, a format A that has x dB larger NLT than B, but also x dB worse sensitivity than B, achieves the same maximum distance.

5. Conclusions

We have shown that in dispersion uncompensated systems where the nonlinear Gaussian assumption holds, the nonlinear interference accumulation rate $1 + \varepsilon$ can also be measured through the nonlinear threshold decrease rate with distance, and we have provided the accumulation rates of the individual self- and cross-channel nonlinear effects, thus corroborating and complementing recent simulation and lab results [8, 11, 13]. We have then shown how the estimated value ε (when all nonlinear effects are taken into account) as well as the 1dB nonlinear threshold can be used to predict the ultimate transmission performance.

Acknowledgments